Brain (2002), **125,** 1105–1115

Human regional cerebral glucose metabolism during non-rapid eye movement sleep in relation to waking

Eric A. Nofzinger,[1] Daniel J. Buysse,[1] Jean M. Miewald,[1] Carolyn C. Meltzer,[1,2] Julie C. Price,[2] Robert C. Sembrat,[2] Hernando Ombao,[4] Charles F. Reynolds, 3rd,[1] Timothy H. Monk,[1] Martica Hall,[1] David J. Kupfer[1] and Robert Y. Moore[1,3]

[1]*Department of Psychiatry,* [2]*Department of Radiology and* [3]*Department of Neurology, University of Pittsburgh School of Medicine and* [4]*Department of Statistics, University of Pittsburgh, PA, USA*

Correspondence to: Eric A. Nofzinger, Department of Psychiatry, University of Pittsburgh School of Medicine, 3811 O'Hara Street, Pittsburgh, PA 15213-2593 USA
E-mail: nofzingerea@msx.upmc.edu

Summary

Sleep is an essential human function. Although the function of sleep has generally been regarded to be restorative, recent data indicate that it also plays an important role in cognition. The neurobiology of human sleep is most effectively analysed with functional imaging, and PET studies have contributed substantially to our understanding of both rapid eye movement (REM) and non-rapid eye movement (NREM) sleep. In this study, PET was used to determine patterns of regional glucose metabolism in NREM sleep compared with waking. We hypothesized that brain structures related to waking cognitive function would show a persistence of function into the NREM sleep state. Fourteen healthy subjects (age range 21–49 years; 10 women, 4 men) underwent concurrent EEG sleep studies and [^{18}F]fluoro-2-deoxy-D-glucose PET scans during waking and NREM sleep. Whole-brain glucose metabolism declined significantly from waking to NREM sleep. Relative decreases in regional metabolism from waking to NREM sleep occurred in wide areas of frontal, parietal, temporal and occipital association cortex, primary visual cortex, and in anterior/dorsomedial thalamus. After controlling for the whole-brain declines in absolute metabolism, relative increases in regional metabolism from waking to NREM were found bilaterally in the dorsal pontine tegmentum, hypothalamus, basal forebrain, ventral striatum, anterior cingulate cortex and extensive regions of the mesial temporal lobe, including the amygdala and hippocampus, and in the right dorsal parietal association cortex and primary somatosensory and motor cortices. The reductions in relative metabolism in NREM sleep compared with waking are consistent with prior findings from blood flow studies. The relative increases in glucose utilization in the basal forebrain, hypothalamus, ventral striatum, amygdala, hippocampus and pontine reticular formation are new observations that are in accordance with the view that NREM sleep is important to brain plasticity in homeostatic regulation and mnemonic processing.

Keywords: amygdala; cerebral glucose metabolism; hippocampus; non-rapid eye movement sleep; prefrontal cortex

Abbreviations: FWHM = full width half maximum; [^{18}F]FDG = [^{18}F]fluoro-2-deoxy-D-glucose; GCRC = General Clinical Research Center; MRDglc = metabolic rate of deoxyglucose; NREM = non-rapid eye movement; REM = rapid eye movement; ROI = region of interest; SPM = statistical parametric mapping

Introduction

Recent studies have emphasized a role for non-rapid eye movement (NREM) sleep in maintaining normal waking cognitive function. Hippocampal ensemble memories have been shown to reactivate during NREM sleep (Wilson and McNaughton, 1994; Sutherland and McNaughton, 2000). In one model of memory trace formation, sharp wave-concurrent population bursts in the hippocampus occurring during slow wave sleep in regions previously activated during waking exploratory behaviour is viewed as an important component of long-term potentiation underlying the formation of memory (Buzsaki, 1989). Cognitive neuroscience studies indicate that NREM sleep plays an important role in

improving performance on visual discrimination tasks (Gais *et al*., 2000; Stickgold *et al*., 2000).

Prior human PET studies of NREM sleep have utilized measurement of cerebral blood flow to show that this behavioural state is associated with altered function in cortical areas involved in waking cognition (Braun *et al*., 1997; Hofle *et al*., 1997; Andersson *et al*., 1998; Kajimura *et al*., 1999; Maquet, 2000). Most studies demonstrated a significant reduction in relative blood flow in thalamus and cortex, particularly in association cortex. These regions are thought to play fundamental roles in waking cognitive function. In general, these studies have been limited by the resolution of PET blood flow analysis, and have not focused on whether there are regions of the brain that may be relatively activated during this state. In part, this is related to the general observation that overall brain function declines during NREM sleep. If there are brain structures that preserve some relative function, or show enhanced function, during NREM sleep, this would be in accordance with the hypothesis that these structures are involved in active processes during NREM sleep that support waking cognitive function.

The current study was designed to elucidate the functional differences between waking and NREM sleep using [^{18}F]fluoro-2-deoxy-D-glucose ([^{18}F]FDG) PET with a region of interest (ROI) and statistical parametric mapping (SPM) analysis. With our method (Nofzinger *et al*., 1998), subject attrition tends to be low as subjects are not required to sleep with their heads immobilized in a scanning device, as is the case in PET blood flow or fMRI studies. [^{18}F]FDG PET also has excellent spatial resolution. Given our interest in defining regions of the brain that may play an active role in the functions of NREM sleep, we also assessed both relative increases and relative decreases in glucose utilization from waking to NREM. We hypothesized that, in addition to confirming prior findings from PET blood flow studies of relative declines in function in thalamus and association cortex in NREM sleep, there would be a relative preservation of function in hypothalamic and basal forebrain structures known to play a role in sleep generation and maintenance, and in temporal lobe regions, particularly the hippocampus, where animal studies have documented a specific function during NREM sleep.

Material and methods

Study design

Fourteen healthy subjects aged <49 years (10 women and 4 men; 1 African American, 13 Caucasian; mean age ± standard deviation, 34.0 ± 9.6 years; right-handed only) participated in the study, which involved three polysomnographically recorded nights of sleep and two [^{18}F]FDG PET scans. Subjects were recruited from the local area via advertising for healthy individuals to participate in sleep research studies. The research study was reviewed and approved by The Review Board of The University of Pittsburgh, and all subjects provided written informed consent to participate. The total pool of subjects entered was 20. Of these, six subjects did not maintain stage 2 NREM sleep for >80% of the [^{18}F]FDG PET uptake period and were excluded from analysis. All subjects were free of medications that could affect mood or sleep for at least 2 weeks prior to EEG sleep and PET studies. Subjects who could not remain drug- or alcohol-free during the study, verified by nightly drug screens, were excluded. Healthy subjects were required to have no personal or family history of major depression according to Research Diagnostic Criteria (RDC; Spitzer *et al*., 1978), or any other psychiatric or sleep disorder including depression, schizophrenia, lifetime history of substance abuse or alcoholism, borderline or antisocial personality disorder, organic affective disorder, schizoaffective disorder, psychotic subtype of major depression or bipolar depression according to Diagnostic and Statistical Manual (DSM)-IV (American Psychiatric Association, 1994) criteria. They were required to have a score of ⩽6 on the first 17 items of the Hamilton Rating Scale for Depression (HRSD) (Hamilton, 1960). Medical histories, physical examinations and laboratory tests were conducted at entry into the study on all subjects who met medical exclusion criteria described previously (Nofzinger *et al*., 1999). Subjective sleep quality was assessed using the Pittsburgh Sleep Quality Index (PSQI; Buysse *et al*., 1989). Any subject with an apnoea/hypopnoea index of ⩾10 on night 1 of screening was excluded from further study.

EEG sleep methods

EEG sleep studies were performed at the General Clinical Research Center (GCRC) of the University of Pittsburgh Medical Center (NIH, RR00056). EEG sleep was monitored on nights 1, 2 and 3. Screening for sleep apnoea was conducted on night 1. Night 2 data were used as baseline EEG sleep data. Subjects reported to the GCRC at 6 p.m. The subjects were asked to go to bed at their 'usual' bedtime, defined as their mean daily sleep-log bedtime over the 7 days preceding sleep studies. On nights 1 and 2, subjects had sham IV tubing taped over their forearms to accommodate an indwelling IV used on night 3. Polysomnographic recordings were conducted according to published criteria from our laboratory (Vasko *et al*., 1997). The EEG sleep montage consisted of a C4/A1-A2 EEG channel, two electrooculograph (EOG) channels (right and left eyes) referenced to linked mastoids, and a sub-mental EMG channel. All electrode impedances were determined to be <5000 Ω. The EEG signal was collected using Grass 7P511 amplifiers. Filter settings for the EEG were 0.3–100 Hz. The EMG was bipolar, with a filter setting of 10–90 Hz. EEG sleep was scored visually by raters blind to clinical information, according to Rechtschaffen and Kales criteria (Rechtschaffen and Kales, 1968). Inter-rater sleep scoring reliability for major sleep variables was checked periodically. Kappa values ranged from 0.76 to 0.85. We have previously

published definitions for visually scored sleep variables (Keshavan *et al*., 1998).

PET methods

Regional cerebral glucose metabolism was assessed during both waking and NREM sleep using the [^{18}F]FDG PET method (Nofzinger *et al*., 1998, 2000). The waking PET study was carried out on the morning following the second night of sleep in the GCRC 2–4 h after awakening. The NREM sleep PET study was performed during the first NREM sleep following at least two undisturbed nights of sleep in the GCRC. PET studies used a 4–6 mCi dose of [^{18}F]FDG PET with the time of injection via an indwelling catheter at either 5–7 min following the identification of the first sleep spindle (nine subjects) or 20 min after sleep onset, which was defined as the first consecutive 10 min of stage 2, 3 or 4 sleep (five subjects). The period of uptake for each of the scans was a 20-min period within the first NREM period of the night. In both the waking and NREM sleep conditions, subjects were monitored by polysomnography so that behavioural state could be determined while they were left undisturbed for 20 min following injection of the radioisotope. For the waking study, subjects were monitored continuously by EEG, and awakened at any sign of sleep. Twenty minutes after radioisotope injection, subjects were placed in a wheelchair, transported to the PET centre and positioned in the PET scanner for a 30-min emission scan (six summed sequential 5-min PET emission scans beginning 60 min after injection of the [^{18}F]FDG PET). This was followed by a 15-min rod-windowed transmission scan. As such, the experimental conditions from 20 min post-injection to the end of scanning were identical between subjects and between conditions (waking and NREM sleep). The use of a low dose of [^{18}F]FDG PET as well as the use of rod-windowing to reduce contamination of the transmission scan from activity in the patient allowed us to perform the transmission scan after the emission scan so as to minimally disrupt the experimental condition up to the emission scanning.

The acquisition protocol included 3D (septa retracted) mode in an ECAT HR+ PET scanner. An individually moulded, thermoplastic head holder (marked with laser guidance for repositioning) was made for each subject to minimize head movement and to allow for head positioning for scanning. The head was positioned such that the lowest scanning plane (visualized by a system of laser lines within the scanner gantry) was parallel to and 1 cm below the canthomeatal line. All PET images were reconstructed using standard commercial software as 63 transaxial slices (each 2.4 mm thick). For images acquired under these conditions, the full width half maximum (FWHM) resolution of a point source in air is ~5 $\pm$ 0.5 mm transverse and 4.5 $\pm$ 0.5 mm axially (Brix *et al*., 1997). The image reconstruction using a Hanning window with cut-off equal to the Nyquist frequency resulted in an estimated (including the effect of scatter) true image FWHM resolution of 7.1 mm in the transverse plane and 6.7 mm axially (P. Kinahan, unpublished data). The broader axial resolution in this case arises from the lack of septa in the HR+ studies, resulting in a degradation of axial resolution by oblique scatter.

MRI methods

Subjects underwent MRI scanning before their first PET study using a Signa 1.5 Tesla scanner (GE Medical Systems, Milwaukee, Wisc., USA). The subjects were positioned in a standard head coil and a brief scout sagittal T_1-weighted image was obtained. Standard axial T_1-weighted (echo time, TE = 18; repetition time, TR = 400; number of excitations, NEX = 1; slice thickness = 3 mm/interleaved; pixel size = 0.9375 mm; 256 $\times$ 256 pixels/section) images were acquired. MRI data were transferred to the PET facility over an electronic network. Pixels that corresponded to the scalp and calvarium were removed from the MRI data so that the eventual MRI mask would remove radioactivity due to these structures when subsequently aligned with the PET data (Sandor and Leahy, 1997). This process was performed using ANALYZE software (Biomedical Imaging Resource, Mayo Foundation, Rochester, Minn., USA) by setting all non-brain voxels to zero intensity.

Image analysis

Image analysis included SPM analyses and MRI-guided whole-brain ROI analyses. The SPM analysis provided whole-brain voxel-by-voxel analyses of differences between the two conditions: waking and NREM sleep. The whole-brain ROI analysis was used to determine the indirect measure of whole-brain metabolism for each PET study. Analyses were carried out using Sun Sparcstation computers (Sun Microsystems Inc., Palo Alto, Calif., USA). All alignments and coregistrations were performed using a modification of R. Woods' automated algorithms for PET-to-PET alignment and PET-to-MRI cross-modality registration as described previously (Woods *et al*., 1992, 1993; Minoshima *et al*., 1993; Wiseman *et al*., 1996; Nofzinger *et al*., 1998). For the MRI-guided whole-brain ROI analysis, each subject's summed PET image was registered to that subject's MRI study. Methods for translating the PET images into a common Talairach space for use in the grouped SPM analyses were as presented previously (Nofzinger *et al*., 1999).

Determination of the whole-brain ROI

For the whole-brain ROI, a brain/non-brain segmentation was applied to the MRI data in order to minimize the dilution of whole-brain metabolic values by the individually variable contribution of CSF spaces. Image processing was performed using routines written in Interactive Data Language (IDL) (Research Systems Inc., Boulder, Col., USA), which were developed and validated at the

Table 1 *Demographic and EEG sleep measures (*n = *14 healthy subjects)*

Measure	Mean	Minimum	Maximum	SD
Age (years)	34.0	21.0	49.0	9.6
Gender	10F/4M			
PSQI total (n = 10)	2.1	1	5	1.3
Sleep latency (min)	10.9	4	17	4.3
Time spent asleep (min)	441.6	371	551	49.0
Sleep efficiency (%)	95.0	87.9	98.2	3.3
% Stage 1	4.5	0.7	11.7	3.0
% Stage 2	61.6	51.5	74.6	8.3
% Stage 3	6.1	0.2	12.1	3.3
% Stage 4	3.6	0.0	11.6	4.5
REM (%)	24.2	17.8	29.5	2.6
REM latency (min)	55.6	1	115	28.2
Whole-night NREM delta power (V^2/Hz)	41.6	17.6	112.2	27.8
NREM PET sleep latency (min)	29.0	5.7	123.0	31.6
NREM PET uptake delta power (V^2/Hz)	58.3	28.9	90.1	21.6

PSQI = Pittsburgh Sleep Quality Index.

University of Pittsburgh PET facility. The segmentation was performed on the subject's MRI study by the selection of an optimal threshold value obtained by fitting pixel signal intensities to Gaussian distributions (Mueller-Gaertner *et al*., 1992) This was accomplished in a semi-automated manner, with a rater providing the range of signal intensity over which the Gaussian curves were fitted. Using this threshold, a binary brain tissue image data set was then created by assigning brain pixels a value of unity and CSF pixels a value of zero. This mask could then be used on the subject's MRI co-registered PET image to assess whole-brain metabolism.

Semi-quantitative measure of the utilization rate of [^{18}F]FDG PET

For the indirect assessment of glucose metabolism alterations in the [^{18}F]FDG PET sleep studies, a modified simplified kinetic method (Hunter *et al*., 1996) was used as an indirect measure of absolute glucose metabolism as described previously (Nofzinger *et al*., 2000). In this approach the plasma integral was estimated from six non-arterialized venous plasma samples collected about every 8 min over 45–95 min after [^{18}F]FDG PET injection. This approach circumvented the problem of arterial cannulation and continuous arterial sampling that may interfere with sleep integrity and contribute to subject attrition. Once the whole-brain ROIs were defined from the MRIs, these ROIs were applied to the co-registered [^{18}F]FDG PET image data set to obtain the C_{PET} values (see below) for each PET image plane (63 planes). The modified simplified kinetic method (see Equation 1 below) was applied on a plane-by-plane and whole-brain basis to measure the metabolic rate of deoxyglucose (MRDglc). In the calculation of MRDglc, no lumped constant value is used.

$$\mathrm{MRDglc} = \frac{C_{PET} \times [\mathrm{Cal\ Factor}]}{\int_0^T C_{p\text{-}FDG}(t)\,dt} \times C_{p\text{-}Glu}\ (\mu\mathrm{mol}/100\,\mathrm{ml}/\mathrm{min})$$

where C_{PET} was the average PET counts/s/pixel that was measured over 60–90 min after [^{18}F]FDG PET injection and the Cal Factor was the PET scanner calibration factor (μCi/ml:PET counts/s/pixel ratio). The plasma concentrations of [^{18}F]FDG PET and glucose are represented by $C_{p\text{-}FDG}$ (μCi/ml) and $C_{p\text{-}Glu}$ (μmol/100 ml), respectively.

Statistical analyses

For differences in whole-brain metabolism between waking and NREM sleep, we used paired t-tests. Analyses were carried out using SPSS software. For differences in relative regional metabolism between waking and NREM, we used Statistical Parametric Mapping, 1999 version (SPM99; Friston *et al*., 1990, 1991). We chose a whole-brain exploratory approach to the data, given that this is the first assessment of NREM metabolism in human subjects using an SPM approach. As revealed below, this approach is very conservative given the similarities in the findings from this report with those from blood flow methods. Prior to statistical analyses, the PET data were co-registered to every subject's MRI, spatially normalized into the Talairach space and finally were smoothed using a Gaussian kernel with FWHM at 10 × 10 × 10 mm. The waking and NREM scans were corrected for global metabolism using analyses of covariance (ANCOVA). Thresholding for grey matter was performed by creation of a mask including voxels with ⩾70% mean counts. Statistic images, which consist of a t-score computed at every voxel, were created for each of the contrasts used in the analysis (waking – NREM > 0, and waking –

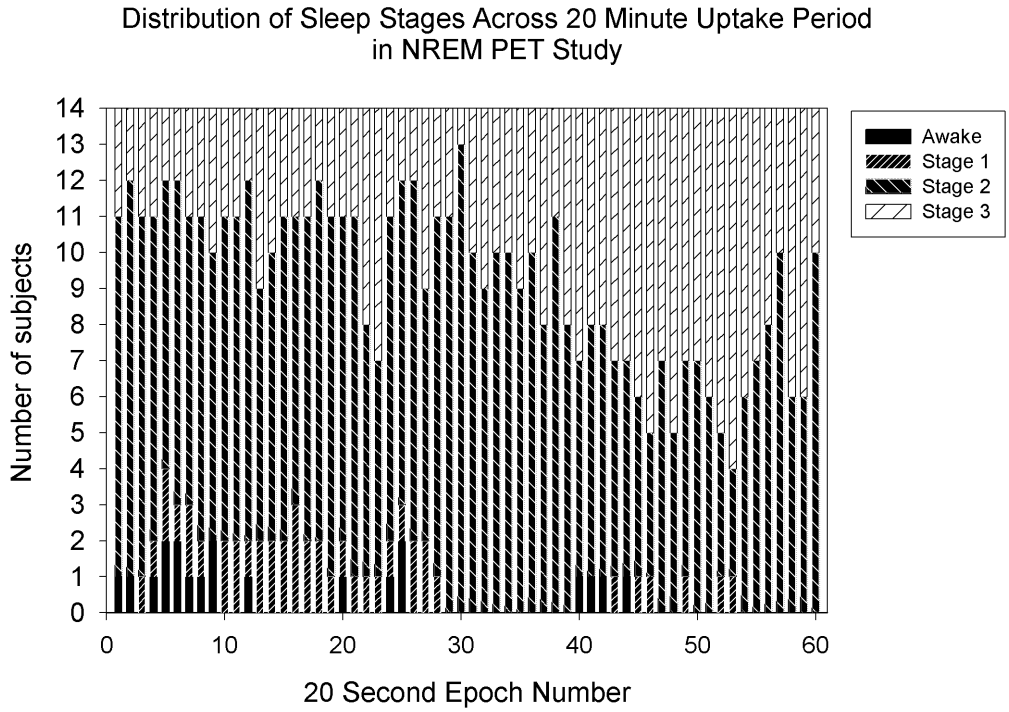

Fig. 1 Minute-by-minute distribution of visually scored sleep stages in the initial 20 min of [^{18}F]FDG uptake and metabolism for the NREM sleep PET scan.

NREM < 0). Local (cluster) statistical maxima were identified by their Talairach atlas (*x*, *y*, *z*) coordinates (Talairach and Tournoux, 1988). In the analysis, we used cluster-level *P*-values that are corrected for multiple comparisons. The voxels were first thresholded at $P < 0.01$ and (de)activation in a cluster is considered significant if its corrected *P*-value is <0.05. As a precaution, by using a cluster level analysis for determining significant effects, we limit our ability to define local maxima spatially within the cluster. Interpretations therefore need to be confined to the entire spatial extent of the cluster activated. In addition to the global analysis, we also applied a volume of interest analysis to the anterior/dorsomedial and ventrolateral thalamus. There are extensive animal data and prior functional brain imaging data indicating that these thalamic regions have lower relative blood flow during NREM sleep than during waking. On this basis, we hypothesized that glucose utilization in these thalamic areas would be significantly reduced from waking to NREM sleep. Given prior information that anterior and dorsomedial thalamic nuclei may be preferentially involved (Kajimura *et al*., 1999), we used both an anterior/dorsomedial ROI and a ventrolateral ROI, which was predicted to be less involved. The reduction was considered to be statistically significant if the corrected *P*-value was <0.01. Anatomic localizations of regions of significance were aided by superimposing the statistic image onto each individual's MRI. Both the statistic image and the MRI had been spatially normalized into the same Talairach coordinates as part of the spatial normalization procedure (described above).

Results

Demographic and EEG sleep measures

Demographic information and results of EEG sleep analyses from undisturbed baseline night 2 of sleep are presented for the group in Table 1. These measures demonstrate that this is a healthy young to mid-life adult group with few sleep complaints and normal EEG sleep.

Distribution of EEG sleep within the NREM [^{18}F]FDG PET uptake period

Figure 1 shows an epoch-by-epoch distribution of EEG sleep staging across the sixty 20-s epochs during the 20-min period when [^{18}F]FDG PET uptake and metabolism is considered greatest. This demonstrates that there were very few arousals over this period and that the resultant sleep stages reflected in the PET acquisition images would reflect predominantly visually scored stage 2 NREM sleep, with some stage 3 and minimal stage 1 sleep. Similar inspection of the data during the waking [^{18}F]FDG PET uptake period revealed no periods of sleep over this time.

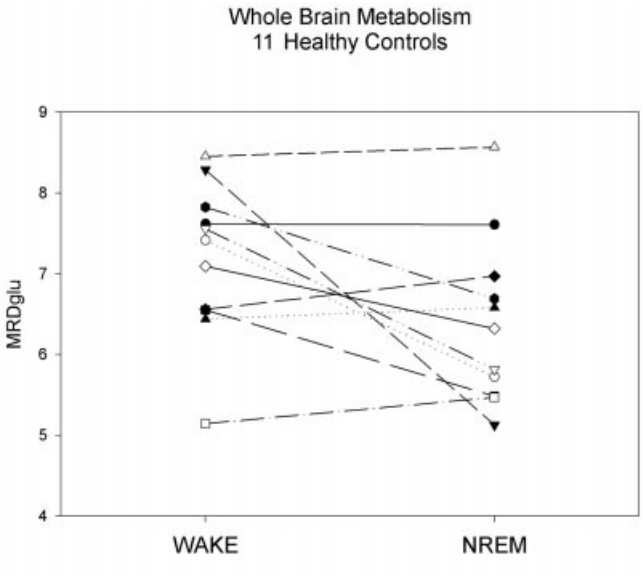

Fig. 2 Individual values for an indirect measure of whole-brain metabolism during waking and NREM sleep.

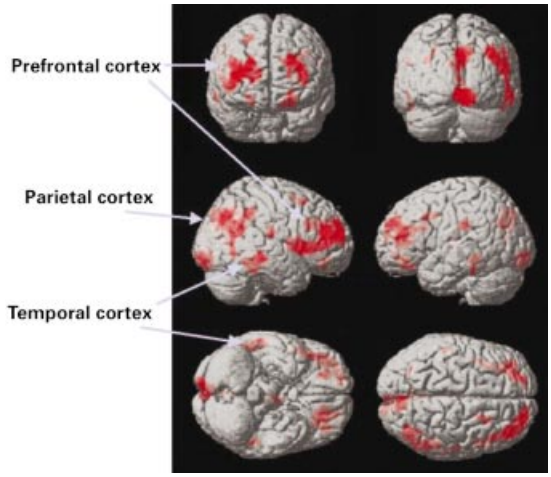

Fig. 3 Three-dimensional rendering of regions demonstrating significantly less relative metabolism during NREM sleep in relation to waking.

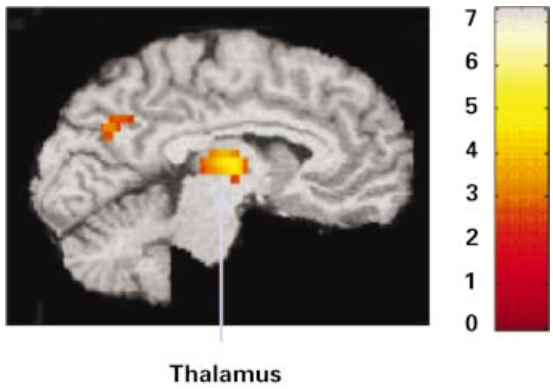

Fig. 4 Sagittal section showing regions of the thalamus that demonstrated significantly less relative metabolism during NREM sleep in relation to during waking ($P < 0.01$). The background brain MRI is from a normal healthy subject and has been spatialized normalized into the same Talairach space as the statistical image.

Relationship between waking and NREM sleep whole-brain metabolism

Figure 2 shows the individual values of an indirect measure of whole-brain glucose metabolism, the MRDglc, during waking and NREM sleep on subjects for whom all data were available for calculation of this measure. In three subjects, blood levels for glucose and radioactivity counts could not be obtained because blood samples could not be collected. The mean ± standard deviation MRDglc for waking and NREM sleep were 7.18 ± 0.96 and 6.40 ± 1.04, respectively—an 11% decrease ($P < 0.02$, two-tailed *t*-test). All subsequent analyses reflect relative regional changes after controlling for these differences in global metabolism.

Reductions in regional relative metabolism from waking to NREM sleep

Figures 3 and 4 show regions where relative metabolism during NREM sleep is less than that during waking. Figure 3 allows for visualization of the larger pattern of decreases across broad regions of cortex in a 3D rendering of the results onto the cortical surface. Table 2 shows structures that demonstrated statistically significant decreases from waking to NREM sleep at the cluster level following correction for multiple comparisons. As seen in Figs 3 and 4, the regions demonstrating this difference included large regions of frontal, parietal, temporal and occipital cortex (Fig. 4). In frontal cortex, these regions included association areas in both dorsolateral prefrontal cortex [Brodmann areas (BA) 44, 45, 46, 8, 9] and ventrolateral prefrontal cortex (BA 11, 47). In the parietal and temporal lobes, the regions included association areas in the angular gyrus and the supramarginal gyrus (BA 39, 40), and in lateral temporal association cortex (BA 21, 20). In the occipital cortex, both primary visual sensory cortex (BA 17) and visual association cortex (BA 18) are included. No statistically significant decreases in relative metabolism were found in the following areas: (i) the brainstem; (ii) primary limbic structures such as amygdala, septal region, hippocampus and cingulate cortex; (iii) paralimbic structures such as the orbitofrontal cortex, insula, temporal pole and parahippocampal cortices; and (iv) primary sensory and motor cortex with the exception of the visual system.

Reductions in regional relative metabolism from waking to NREM sleep in the thalamus

Using the volume of interest approach, relative metabolism declined in NREM sleep in the anterior/dorsomedial region of

Table 2 *Decreases in relative regional metabolism from waking to NREM sleep (*n = *14 healthy subjects)*

Region	Cluster level *P*-value (corrected)	Number of voxels significant at $P < 0.01$	Maximum voxel level T in cluster	Talairach *x*, *y*, *z*
Right dorsolateral prefrontal cortex	<0.001	1048	7.27	46, 14, 0
Visual cortex	0.011	315	5.61	6, –92, –12
Right parietal cortex	<0.001	513	5.56	38, –72, 36
Left dorsolateral prefrontal cortex	<0.001	613	5.44	–30, 32, 24
Parietal cortex	0.002	435	4.61	8, –78, 32

Table 3 *Increases in relative regional metabolism from waking to NREM sleep (*n = *14 healthy subjects)*

Region	Cluster level *P*-value (corrected)	Number of voxels significant at $P < 0.01$	Maximum voxel level T in cluster	Talairach *x*, *y*, *z*
R fusiform gyrus	<0.001	528	7.84	24, –72, –12
R superior parietal cortex	0.037	245	6.38	20, –62, 40
R primary sensory motor cortex	<0.001	541	6.06	28, –32, 40
L hippocampus; L amygdala; L hypothalamus/basal forebrain	<0.001	1230	5.56	–36, –36, –8
Dorsal pontine tegmentum; L subgenual anterior cingulate; R anterior hypothalamus/R basal forebrain; R amygdala; R hippocampus	<0.001	1337	5.42	–8, 34, 4
L fusiform gyrus	0.040	240	4.88	–24, –70, –16
R dorsal anterior cingulate	0.002	407	4.67	4, 4, 28

R = right; L = left.

the thalamus (maximum *Z* statistic = 3.71 at a region of 5-mm radius centred on Talairach coordinates $x = -5$, $y = -12$, $z = 10$; corrected *P*-value = 0.003). Relative metabolism was not significantly different at the $P < 0.01$ level in the ventrolateral region of the thalamus (maximum *Z* statistic = 2.76 at a region of 5-mm radius centred on Talairach coordinates $x = -14$, $y = -16$, $z = 4$; corrected *P*-value = 0.072).

Increases in regional relative metabolism from waking to NREM sleep

Table 3 and Figs 5 and 6 show regions where relative metabolism increased from waking to NREM sleep. These findings should be understood to reflect relative regional change following correction for the decline in whole-brain metabolism from waking to NREM sleep. An increase in relative metabolism was noted in isolated areas of association and primary sensory motor cortex including: (i) a large extent of visual association cortex in the fusiform gyrus, bilaterally (BA 19) in the occipital cortex; (ii) the right superior parietal cortex (BA 7); and (iii) right primary somatosensory and motor cortex. In addition, large confluent areas of increased relative metabolism during NREM sleep were noted bilaterally in mesial temporal lobe (hippocampus and amygdala; see Fig. 5), hypothalamus, basal forebrain and ventral striatum (see Fig. 6). Increased relative metabolism was noted in the subgenual region of the anterior cingulate cortex (BA 25), a small region of the right dorsal anterior cingulate (BA 24) and in pontine reticular formation.

Discussion

This study demonstrates changes in whole brain and regional brain glucose metabolism between wakefulness and NREM sleep in healthy young adult humans. Globally, cerebral glucose metabolism declines from waking to NREM sleep. Regionally, greater reductions occur in broad regions of frontal, parietal, temporal and occipital cortex and in the anterior/dorsomedial region of the thalamus. Relative increases in regional metabolism were noted in the dorsal pontine tegmentum, the basal forebrain, the hypothalamus, ventral striatum, anterior cingulate cortex, and in amygdala and hippocampal formation. The general pattern of reductions in metabolism from waking to NREM sleep is consistent with animal studies of NREM sleep and with prior human functional neuroimaging studies using PET blood flow methods. The regional pattern of brain structures showing increased relative metabolism in NREM sleep is consistent with animal studies demonstrating hypothalamic and basal forebrain participation in the generation and maintenance of NREM sleep, and mesial temporal lobe structures role in mnemonic processing in NREM sleep. Nevertheless, given the novelty of the pattern of relative increase in metabolism from waking to NREM sleep, we feel it is important now to

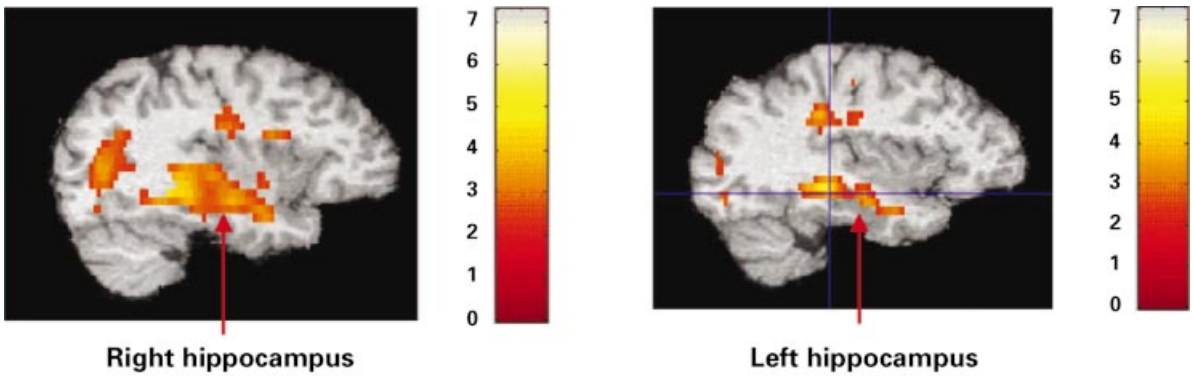

Fig. 5 Sagittal sections showing regions of the hippocampus (left and right) that demonstrated significantly greater relative metabolism during NREM sleep in relation to during waking ($P < 0.01$). The background brain MRI is from a normal healthy subject and has been spatialized normalized into the same Talairach space as the statistical image.

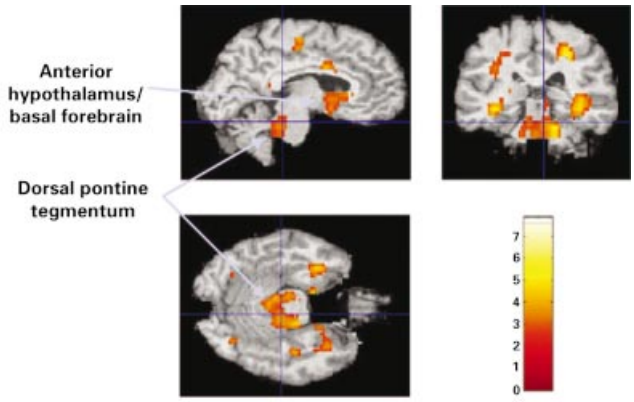

Fig. 6 Brain sections showing regions of the dorsal pontine tegmentum, and the hypothalamus/basal forebrain area that demonstrated significantly greater relative metabolism during NREM sleep in relation to waking ($P < 0.01$). The background brain MRI is from a normal healthy subject and has been spatialized normalized into the same Talairach space as the statistical image.

replicate these findings in a new group of subjects using a more focused ROI approach.

Can these results be compared with those obtained using blood flow methods?

Whereas energy metabolism related to neuronal activity in the brain relies almost completely on glucose, there is generally a coupling of cerebral blood flow and glucose metabolism sufficient to warrant direct comparisons of [^{18}F]FDG and $H_2{}^{15}O$ PET studies (e.g. Jueptner and Weiller, 1995). Cerebral blood flow methods offer better temporal resolution (1–2 min) and can be repeated across a single night of sleep. The primary limitation is that this method requires immobilization of the head for scanning during sleep, potentially limiting natural sleep and leading to high rates of subject attrition. Moreover, [^{18}F]FDG PET has a better spatial resolution than the blood flow method. If the glucose metabolic method employed in this study, which has lower rates of subject attrition, provides comparable findings, then [^{18}F]FDG PET studies could be applied to the study of human patient populations, where minimization of subject attrition is important. There is a further concern that the sleep obtained in the scanner, as is necessary with rCBF analysis, may not be as natural as normal sleep in a bed. The general consistency between the regions found to have relative reductions in function from waking to NREM sleep in the current study and in those using blood flow methods indicates that both methods accurately define regional changes in brain function in NREM sleep.

Glucose metabolism in the hippocampus showed a striking bilateral increase from waking to NREM sleep. Hippocampal neurone ensembles have been shown to reactivate during NREM sleep in patterns that are very similar to ones activated during waking learning (Wilson and McNaughton, 1994; Sutherland and McNaughton, 2000). In one model of memory trace formation, sharp wave-concurrent population bursts in the hippocampus occurring during slow-wave sleep in regions previously activated during waking exploratory behaviour is viewed as an important component of long-term potentiation underlying the consolidation of memory (Buzsaki, 1989). Hirase *et al*. (2001), however, have shown that the changes in hippocampal neuronal activity from waking to NREM sleep are not related to the mean level of firing but rather to the pattern of firing across states. Other studies suggest a role for NREM sleep in improving performance on visual discrimination tasks (Gais *et al*., 2000; Stickgold *et al*., 2000). These lines of evidence suggest a role for NREM sleep in general and for hippocampal activity, in particular a role in mnemonic processes. The relationships between the increased relative metabolism in the hippocampus observed in NREM sleep in the current study and any specific function in memory formation, however, remain to be clarified.

How do the current results in the hypothalamus and limbic areas relate to prior studies? Kajimura *et al*. (1999) studied blood flow in both light and deep NREM sleep. They did not find any significant changes in either absolute or relative blood flow between waking and either light or deep sleep in

the amygdala, the hippocampus or the basal forebrain. Hofle *et al*. (1997) studied the relationship between delta sleep and blood flow. They did not find any statistically significant relationship between delta sleep and relative blood flow in the hippocampus, amygdala or basal forebrain. Maquet *et al*. (1997) studied blood flow as a correlate of slow-wave sleep versus either waking or REM sleep. A negative correlation was found with relative blood flow in the right mesial temporal cortex (amygdala, parahippocampal and entorhinal cortex) and in the basal forebrain. Andersson *et al*. (1998) studied blood flow during NREM sleep in relation to waking. They found reduced blood flow in the amygdala and bilaterally in the hippocampus. No statistically significant change was noted in the basal forebrain. Braun *et al*. (1997) studied blood flow during NREM sleep in relation to both pre- and post-sleep waking. They did not demonstrate any NREM sleep-related decline in either the hippocampus or the amygdala. This was in contrast to declines in other paralimbic regions. They interpreted this persistence of blood flow during NREM sleep in contrast to other paralimbic structures as a disconnect of these structures within NREM sleep. Reductions in blood flow were noted during NREM sleep in the basal forebrain, anterior hypothalamus–preoptic area. Finally, Kennedy *et al*. (1982) studied glucose metabolism using the [2-^{14}C]deoxyglucose method in the rhesus monkey during waking and NREM sleep. Whereas they found global declines in absolute metabolism throughout the brain during NREM sleep, an inspection of their individual data suggests that there were relative increases in function from waking to NREM sleep in the lateral amygdala (waking versus NREM relative metabolism = 0.89 versus 1.0); the basal amygdala (0.77 versus 0.88); the hippocampus (0.97 versus 1.12); the nucleus accumbens (1.0 versus 1.16); and in a summed measure of their subregions of the hypothalamus (0.95 versus 1.03). Based on these studies it is difficult to generalize whether there are consistent changes in relative regional brain function from waking to NREM sleep in these limbic structures and in the basal forebrain/hypothalamus area. If anything, the changes observed in these regions are much less consistent than the relative declines in function noted in heteromodal association cortex and in the thalamus across all studies. This leaves open the possibility, as suggested by the results of the current study, that a persistence of relative function in these structures into sleep may signify an important functional role of these structures during sleep.

Cerebral cortex

Consistent with previous reports (Braun *et al*., 1997; Hofle *et al*., 1997; Maquet *et al*., 1997; Andersson *et al*., 1998; Kajimura *et al*., 1999), the largest reductions in cortical regions were observed in frontal, parietal and temporal association cortex, with relative sparing of changes in primary sensory motor cortex. These structures are known to subserve many of the 'on-line' functions necessary for individuals to interact immediately with their environment. The restorative function of NREM sleep, therefore, could preferentially affect cortical regions that are involved in higher order processing.

Potential implications

These glucose metabolic findings support the notion that NREM sleep is critical to waking cognitive function and adaptive behaviour. Notably, thalamocortical loops primarily involving heteromodal association cortex show consistent alterations between waking and NREM sleep in both the current study and in studies using blood flow methodology. Intriguingly, the new finding in this study of a bilateral relative increase in function during NREM sleep in the hippocampus, basal forebrain and anterior hypothalamus raises the possibility that NREM sleep plays some role in overall cognitive function.

Acknowledgements

The authors wish to thank the technical staff of the Clinical Neuroscience Research Center, the General Clinical Research Center and the PET Center at the University of Pittsburgh Medical Center for their help in conducting this work; Irma Ilustre and Tom Carey for help in study coordination; and the anonymous referees for their constructive comments. This research was supported in part by grants MH01414, MH61566, MH62298, MH30915, NIMH37869, RR00056, MH24652 and MH52247.

References

American Psychiatric Association: Diagnostic and statistical manual of mental disorders (DSM-IV). 4th American Psychiatric Association, Washington DC 1994.

Andersson JL, Onoe H, Hetta J, Lidstrom K, Valind S, Lilja A, et al. Brain networks affected by synchronized sleep visualized by positron emission tomography. J Cereb Blood Flow Metab 1998; 18: 701–15.

Braun AR, Balkin TJ, Wesenten NJ, Carson RE, Varga M, Baldwin P, et al. Regional cerebral blood flow throughout the sleep-wake cycle. An H2(15)O PET study. Brain 1997; 120: 1173–97.

Brix G, Zaers J, Adam LE, Bellemann ME, Ostertag H, Trojan H, et al. Performance evaluation of a whole-body PET scanner using the NEMA protocol. National Electrical Manufacturers Association. J Nucl Med 1997; 38: 1614–23.

Buchsbaum MS, Gillin JC, Wu J, Hazelett E, Sicotte N, Dupont RM, et al. Regional cerebral glucose metabolic rate in human sleep assessed by positron emission tomography. Life Sci 1989; 45: 1349–56.

Buysse DJ, Reynolds CF 3rd, Monk TH, Berman SR, Kupfer DJ. The Pittsburgh Sleep Quality Index (PSQI): A new instrument for psychiatric practice and research. Psychiatry Res 1989; 28: 193–213.

Buzsaki G. Two-stage model of memory trace formation: A role for 'noisy' brain states. [Review]. Neuroscience 1989; 31: 551–70.

Friston KJ, Frith CD, Liddle PF, Dolan RJ, Lammertsma AA, Frackowiak RS. The relationship between global and local changes in PET scans. J Cereb Blood Flow Metab 1990; 10: 458–66.

Friston KJ, Frith CD, Liddle PF, Frackowiak RS. Comparing functional (PET) images: the assessment of significant change. J Cereb Blood Flow Metab 1991; 11: 690–9.

Gais S, Plihal W, Wagner U, Born J. Early sleep triggers memory for early visual discrimination skills. Nat Neurosci 2000; 3: 1335–9.

Gerashchenko D, Matsumura H. Continuous recordings of brain regional circulation during sleep/wake state transitions in rats. Am J Physiol 1996; 270: R855–63.

Greisen G, Hellstrom-Vestas L, Lou H, Rosen I, Svenningsen N. Sleep–waking shifts and cerebral blood flow in stable preterm infants. Pediatr Res 1985; 19: 1156–9.

Hamilton M. A rating scale for depression. J Neurol Neurosurg Psychiatry 1960; 23: 56–62.

Heiss WD, Pawlik G, Herholz K, Wagner R, Wienhard K. Regional cerebral glucose metabolism in man during wakefulness, sleep, and dreaming. Brain Res 1985; 327: 362–6.

Hirase H, Leinekugel X, Czurko A, Csicsvari J, Buzsaki G. Firing rates of hippocampal neurons are preserved during subsequent sleep episodes and modified by novel awake experience. Proc Natl Acad Sci USA 2001; 98: 9386–90.

Hofle N, Paus T, Reutens D, Fiset P, Gotman J, Evans AC, et al. Regional cerebral blood flow changes as a function of delta and spindle activity during slow wave sleep in humans. J Neurosci 1997; 17: 4800–8.

Hunter GJ, Hamberg LM, Alpert NM, Choi NC, Fischman AJ. Simplified measurement of deoxyglucose utilization rate. J Nucl Med 1996; 37: 950–5.

Ingvar DH, Rosen I, Johannesson G. EEG related to cerebral metabolism and blood flow. Pharmakopsychiatr Neuropsychopharmakol 1979; 12: 200–9.

Jueptner M, Weiller C. Review: does measurement of regional cerebral blood flow reflect synaptic activity? Implications for PET and fMRI. [Review]. Neuroimage 1995; 2: 148–56.

Kajimura N, Uchiyama M, Takayama Y, Uchida S, Uema T, Kato M, et al. Activity of midbrain reticular formation and neocortex during the progression of human non-rapid eye movement sleep. J Neurosci 1999; 19: 10065–73.

Kennedy C, Gillin JC, Mendelson W, Suda S, Miyaoka M, Ito M, et al. Local cerebral glucose utilization in non-rapid eye movement sleep. Nature 1982; 297: 325–7.

Keshavan MS, Reynolds CF, Miewald JM, Montrose DM, Sweeney JA, Vasko RC, et al. Delta sleep deficits in schizophrenia: evidence from automated analyses of sleep data. Arch Gen Psychiatry 1998; 55: 443–8.

Madsen PL, Schmidt JF, Wildschiodtz G, Friberg L, Holm S, Vorstrup S, et al. Cerebral oxygen metabolism and cerebral blood flow in humans during deep and rapid-eye-movement sleep. J Appl Physiol 1991; 70: 2597–601.

Magnes J, Moruzzi G, Pompeiano O. Synchronization of the EEG produced by low-frequency electrical stimulation of the region of the solitary tract. Arch Ital Biol 1961; 99: 33.

Maquet P. Functional neuroimaging of normal human sleep by positron emission tomography. [Review]. J Sleep Res 2000; 9: 207–31.

Maquet P, Dive D, Salmon E, Sadzot B, Franco G, Poirrier R, et al. Cerebral glucose utilization during sleep-wake cycle in man determined by positron emission tomography and [18F]2-fluoro-2-deoxy-D-glucose method. Brain Res 1990; 513: 136–43.

Maquet P, Degueldre C, Delfiore G, Aerts J, Peters JM, Luxen A, et al. Functional neuroanatomy of human slow wave sleep. J Neurosci 1997; 17: 2807–12.

Meyer JS, Ishikawa Y, Hata T, Karacan I. Cerebral blood flow in normal and abnormal sleep and dreaming. Brain Cogn 1987; 6: 266–94.

Minoshima S, Koeppe RA, Mintun MA, Berger KL, Taylor SF, Frey KA. Automated detection of the intercommissural line for stereotactic localization of functional brain images. J Nucl Med 1993; 34: 322–9.

Moore RY, Abrahamson EA, Van Den Pol A. The hypocretin neuron system: an arousal system in the human brain. Arch Ital Biol 2001; 139: 195–205.

Mueller-Gaertner HW, Links JM, Prince JL, Bryan RN, McVeigh E, Leal JP, et al. Measurement of radiotracer concentration in brain gray matter using positron emission tomography: MRI-based correction for partial volume effects. J Cereb Blood Flow Metab 1992; 12: 571–83.

Nakamura RK, Kennedy C, Gillin JC, Suda S, Ito M, Storch FI, et al. Hypnogenic center theory of sleep: no support from metabolic mapping in monkeys. Brain Res 1983; 268: 372–6.

Nofzinger EA, Mintun MA, Price J, Meltzer CC, Townsend D, Buysse DJ, et al. A method for the assessment of the functional neuroanatomy of human sleep using FDG PET. Brain Res Brain Res Protoc 1998; 2: 191–8.

Nofzinger EA, Nichols TE, Meltzer CC, Price J, Steppe DA, Miewald JM, et al. Changes in forebrain function from waking to REM sleep in depression: preliminary analyses of [18F]FDG PET studies. [Review]. Psychiatry Res 1999; 91: 59–78.

Nofzinger EA, Price JC, Meltzer CC, Buysse DJ, Villemagne VL, Miewald JM, et al. Towards a neurobiology of dysfunctional arousal in depression: the relationship between beta EEG power and regional cerebral glucose metabolism during NREM sleep. Psychiatry Res 2000; 98: 71–91.

Ramm P, Frost BJ. Cerebral and local cerebral metabolism in the cat during slow wave and REM sleep. Brain Res 1986; 365: 112–24.

Rechtschaffen A, Kales A. A manual of standardized terminology, techniques and scoring system for sleep stages of human subjects. NIH Publication No. 204. Bethesda (MD): US Department of Health, Education, and Welfare; 1968.

Sakai F, Meyer JS, Karacan I, Derman S, Yamamoto M. Normal human sleep: regional cerebral hemodynamics. Ann Neurol 1980; 7: 471–8.

Sandor S, Leahy R. Surface-based labeling of cortical anatomy using a deformable atlas. IEEE Trans Med Imaging 1997; 16: 41–54.

Sherin JE, Elmquist JK, Torrealba F, Saper CB. Innervation of histaminergic tuberomammillary neurons by GABAergic and galaninergic neurons in the ventrolateral preoptic nucleus of the rat. J Neurosci 1998; 18: 4705–21.

Shiromani PJ, Scammell T, Sherin JE, Saper CB. Hypothalamic regulation of sleep. In: Lydic R, Baghdoyan HA, editors. Handbook of behavioral state control: cellular and molecular mechanisms. Boca Raton (FL): CRC Press; 1999. p. 311–25.

Spitzer RL, Endicott J, Robins E. Research diagnostic criteria: rationale and reliability. Arch Gen Psychiatry 1978; 35: 773–82.

Steriade M, Iosif G, Apostol V. Responsiveness of thalamic and cortical motor relays during arousal and various stages of sleep. J Neurophysiol 1969; 32: 251–65.

Stickgold R, Whidbee D, Schirmer B, Patel V, Hobson JA. Visual discrimination task improvement: a multi-step process occurring during sleep. J Cogn Neurosci 2000; 12: 246–54.

Sutherland GR, McNaughton B. Memory trace reactivation in hippocampal and neocortical neuronal ensembles. [Review]. Curr Opin Neurobiol 2000; 10: 180–6.

Szymusiak R. Magnocellular nuclei of the basal forebrain: substrates of sleep and arousal regulation. [Review]. Sleep 1995; 18: 478–500.

Talairach J, Tournoux P. Co-planar stereotaxic atlas of the human brain. Stuttgart: Thieme; 1988.

Townsend RE, Prinz PN, Obrist WD. Human cerebral blood flow during sleep and waking. J Appl Physiol 1973; 35: 620–5.

Vasko RC, Brunner DP, Monahan JP, Doman J, Boston JR, el-Jaroudi A, et al. Power spectral analysis of EEG in a multiple-bedroom, multiple-polygraph sleep laboratory. Int J Med Inf 1997; 46: 175–84.

Wilson MA, McNaughton BL. Reactivation of hippocampal ensemble memories during sleep. Science 1994; 265: 676–9.

Wiseman MB, Nichols TE, Dachille MA, Mintun MA. Working towards an automatic and accurate method for PET-MR alignment. J Nucl Med 1996; 37: 224P.

Woods RP, Cherry SR, Mazziotta JC. Rapid automated algorithm for aligning and reslicing PET images. J Comput Assist Tomogr 1992; 16: 620–33.

Woods RP, Mazziotta JC, Cherry SR. MRI-PET registration with automated algorithm. J Comput Assist Tomogr 1993; 17: 536–46

Received August 15, 2001. Revised November 6, 2001.
Second revision December 14, 2001. Accepted December 17, 2001